Research Article | Vol. 27, No. 24 / 25 November 2019 / Optics Express 34952
Optics EXPRESS

Quantitative amplitude measuring φ-OTDR using multiple uncorrelated Rayleigh backscattering realizations

BRANDON REDDING,* MATTHEW J. MURRAY, ALLEN DAVIS, AND CLAY KIRKENDALL

Optical Sciences Division, U.S. Naval Research Laboratory, 4555 Overlook Ave. SW, Washington, D.C. 20375, USA
brandon.redding@nrl.navy.mil

Abstract: We propose and demonstrate a technique to perform quantitative strain sensing using the amplitude of the Rayleigh backscattered light in a modified φ-OTDR system. While standard amplitude measuring φ-OTDR sensors can identify the presence of strain, they cannot perform quantitative measurements because the amplitude of the Rayleigh backscattered light exhibits a non-linear and unpredictable strain response. Here, we demonstrate a technique to computationally recover a linear strain response from a set of uncorrelated Rayleigh backscattering measurements. Using a combination of frequency and polarization multiplexing, we constructed a φ-OTDR system capable of recording 18 uncorrelated Rayleigh backscattering measurements in parallel. By combining information from these 18 measurements, the sensor achieves a linear strain response with total harmonic distortion below −35 dB. The sensor is immune to signal fading, has a minimum detectable strain of 5 $p\varepsilon/\sqrt{Hz}$ and a bandwidth of 500 kHz.

1. Introduction

Fiber optic sensors are able to perform distributed strain measurements over large distances. Rayleigh and Brillouin sensors are particularly attractive due to their ability to use commercial off-the-shelf fiber. While Brillouin sensors are capable of measuring the absolute strain in the fiber, Rayleigh sensors are more commonly used for dynamic strain measurements [1]. One of the most widely adopted sensing architectures based on Rayleigh scattering is phase-sensitive optical time domain reflectometry (φ-OTDR) which has been used in applications including structural health monitoring [1], intrusion detection [2], and pipeline monitoring [3]. The majority of φ-OTDR systems can be divided into two groups: amplitude measuring and phase measuring systems. Amplitude measuring φ-OTDR systems can detect the presence of strain, but since the amplitude of the Rayleigh Backscattering (RBS) signal has a non-linear strain dependence, they cannot provide a quantitative strain measurement [1]. In contrast, the optical phase accumulated over a length of fiber *is* proportional to strain [4], allowing phase measuring φ-OTDR systems to perform quantitative strain measurements. While there are a number of phase measuring φ-OTDR architectures [1,5–7], they all rely on measuring the relative phase between light backscattered from two "reflector regions" in the fiber and a linear response is only guaranteed under the assumption that these reflector regions do not experience strain themselves [1,8,9]. In order to satisfy this requirement, phase measuring φ-OTDR systems tend to use short optical pulses to minimize the reflector size at the cost of reducing the RBS light level—a trade-off which can limit the sensor noise floor. In addition, phase measuring φ-OTDR systems are susceptible to interference fading, although this can be mitigated by using multiple input frequencies [10,11].

To address some of these limitations, a few recent works introduced techniques that enable quantitative strain sensing based on the amplitude of the RBS signal [12–18]. These approaches measure the RBS amplitude as a function of the optical input frequency to construct a RBS

#379674 https://doi.org/10.1364/OE.27.034952
Journal © 2019 Received 10 Oct 2019; revised 1 Nov 2019; accepted 1 Nov 2019; published 14 Nov 2019

Optics EXPRESS

spectrum. Since a change in strain or temperature will introduce a frequency shift in the RBS spectrum [14], quantitative strain information can be extracted by monitoring the evolution of the RBS spectrum. In contrast to phase-measuring φ-OTDR, these techniques are able to extract the algebraic sign of the strain based on the direction of the frequency shift [12,13]. In the most straightforward implementation, the RBS spectrum is measured in series by injecting pulses one frequency at a time [12–15]. However, this approach limits the available sensor bandwidth, prompting researchers to develop chirped pulse techniques which maintain the maximum bandwidth allowed by the round-trip time in the fiber at the cost of increased system complexity [16–18].

In this work, we present a new approach to perform quantitative amplitude measuring φ-OTDR with sensor bandwidth limited only by the roundtrip fiber length. Our approach relies on computationally recovering a linear strain response from a series of uncorrelated RBS patterns. We use a strain recovery algorithm that was recently developed to enable quantitative strain sensing in multimode fiber φ-OTDR [19]. In a multimode fiber, the different spatial modes provide the uncorrelated RBS measurements used to reconstruct the strain [19]. However, the frame rate of the camera used to record the RBS speckle pattern in the multimode fiber system limited the number of sensors which could be measured in parallel. Here, we use a combination of frequency and polarization multiplexing in a single mode fiber to record 18 uncorrelated RBS patterns in parallel from each position in the fiber. We demonstrate a linear strain response with total harmonic distortion of -35 dB, a sensor bandwidth of 500 kHz (dictated by the roundtrip fiber length) and a minimum detectable strain of 5 p$\varepsilon/\sqrt{\text{Hz}}$. We also present simulations evaluating the influence of the number of uncorrelated measurements on the minimum detectable strain and the linearity of the measurement.

2. Operating principle

Figure 1 shows a schematic of a standard phase measuring φ-OTDR sensor along with the quantitative amplitude measuring φ-OTDR sensor proposed in this work. In the phase measuring system, the strain in the sensor region is proportional to the relative phase between light scattered from two reflector regions. In contrast, in our amplitude measuring φ-OTDR, the reflector region and the sensor region are the same. This enables us to use longer pulses than a typical phase measuring φ-OTDR system with the same sensor size and thus collect more light since the RBS power is proportional to the pulse duration [20]. An alternative approach to enable the use of longer pulses without compromising spatial resolution was recently proposed based on chirped pulses and correlation based processing, although these techniques can be susceptible to cross-talk [18,21].

In this work, we obtain a series of uncorrelated RBS measurements of a strain event by using an optical frequency comb as the input pulse. Our sensor is then designed to measure the RBS amplitude of each comb tooth over time, as shown in Fig. 1(b). We then computationally reconstruct the underlying strain from the evolution of the different comb teeth using an algorithm developed in the context of multimode fiber φ-OTDR [19]. Although this work uses uncorrelated RBS measurements at different frequencies instead of measurements of different spatial modes, they still follow Rayleigh statistics allowing us to apply the same algorithm.

While Fig. 1 illustrates the process for one sensor position, fully distributed sensing is achieved by time-gating the RBS light to measure the RBS comb at each position in the fiber. The strain can then be computationally recovered at each position.

Optics EXPRESS

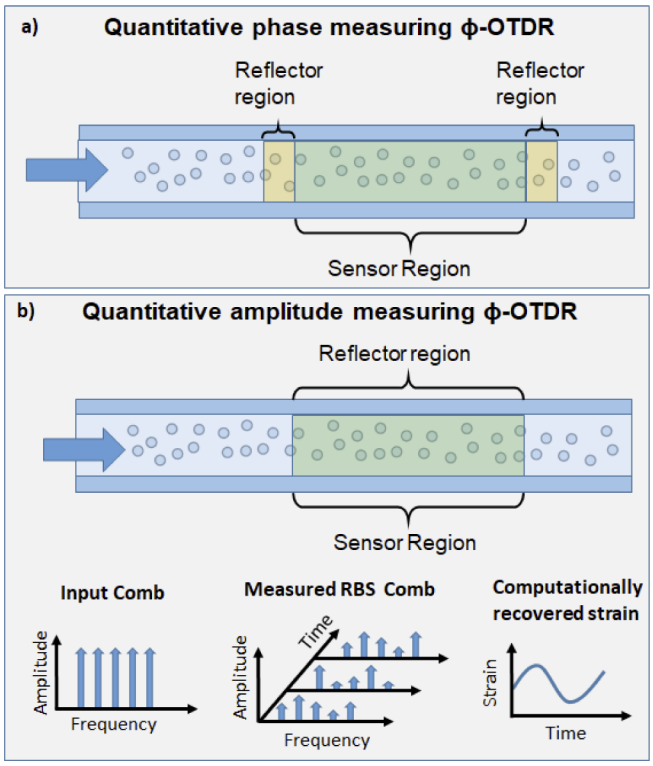

Fig. 1. (a) In a quantitative phase-measuring φ-OTDR system, strain in the sensor region is proportional to the relative phase between light back-scattered from two reflector regions. (b) In the quantitative amplitude measuring φ-OTDR system presented in this work, the reflector region and the sensor region are the same. The input pulse consists of multiple frequency components and the amplitude of each frequency component is measured over time. The strain experienced in the sensor region is then computationally recovered from the evolution of the measured RBS comb.

3. Simulated sensor performance

We first conducted simulations to evaluate the impact of the number of uncorrelated RBS patterns measured on the sensor linearity and noise floor. We used a standard impulse response model [22] to calculate the RBS field, E, as a function of input frequency, ν:

$$E(\nu, t) = \sum_{n=1}^{N} r_n \exp[i2\pi\nu t + i2\beta_\upsilon(z_n + \xi\varepsilon(t)z_n)]\, rect\left(\frac{t-\tau}{T}\right) \tag{1}$$

where r_n is a measure of the reflectivity of the n^{th} scattering center, β_ν is the propagation constant at frequency ν, z_n is the position of the n^{th} scatterer, ξ is the elasto-optic coefficient, ε is the time-varying axial strain, t is time, τ is the temporal delay to the desired sensor region within the fiber, and T is the pulsewidth of the incident light. We calculated the RBS field for 128 input frequencies in 60 MHz steps starting at 193.5 THz (corresponding to a wavelength of ~1550 nm). The pulse duration was set to 100 ns providing a 10 m sensor size. We calculated the RBS field over 10^4 pulses at a pulse repetition rate of 1 MHz under a 10 kHz sinusoidal strain with an amplitude of 50 nε.

Optics EXPRESS

In order to include the influence of shot noise, we assumed the input pulse had a peak power of 1 W and calculated the RBS power, P_{RBS}, as [20]

$$P_{RBS}(z) = P_{in}\left(\frac{v_g T}{2}\right)\alpha_R S\, e^{-2\alpha z} \tag{2}$$

Where P_{in} is the peak power of the input pulse, v_g is the group velocity, α_R is the Rayleigh backscattering coefficient, S is the capture fraction, α is the fiber attenuation, and z is the distance to the sensor. We then calculated the intensity we would expect to measure at each frequency as:

$$I_{measured}(\upsilon, t) = E(\upsilon, t)\cdot E(\upsilon, t)^{*} + \sigma_{SN} \tag{3}$$

The shot noise term, σ_{SN}, is a normally distributed random value with standard deviation equal to $\frac{P_{RBS}\eta T}{h\nu}\frac{1}{N_{freq}}$ where η is the quantum efficiency of the detector and N_{freq} is the number of frequency components in the input comb. This assumes we are able to distribute the RBS light among N_{freq} components and make a shot noise limited measurement of each frequency component (e.g. by using a strong reference arm). We then used the strain recovery algorithm described in [19] to extract the sinusoidal strain using an increasing number of frequency components. Note that the shot noise was adjusted as we increased the number of frequency components according to Eq. 3.

The time varying RBS intensity of four frequency components is shown in Fig. 2(a). By combining information from multiple frequency components, we are able to recover the sinusoidal strain signal, as shown in Fig. 2(b). Note that the "measured" RBS intensity calculated in Eq. 3 was normalized to have a mean value of unity. By providing the strain recovery algorithm with the RBS intensity in normalized units, we can use a single calibration to convert the recovered signal to units of strain [19].

To quantitatively evaluate the impact of the number of frequency components provided to the algorithm, we calculated the strain amplitude spectral density (ASD) as shown in Fig. 2(c) along with the total harmonic distortion (THD). The THD provides a measure of the linearity of the sensor and is defined (in dB) as $THD = 20\log_{10}[(\varepsilon_{2f_{sig}}^2 + \varepsilon_{3f_{sig}}^2 + \varepsilon_{4f_{sig}}^2 + \cdots)^{1/2}/\varepsilon_{f_{sig}}]$ where $\varepsilon_{f_{sig}}$ is the strain at frequency f_{sig}.

We repeated the simulation for 1000 ensembles of randomly distributed scattering centers to produce the plots in Fig. 2(d) which show the minimum detectable strain and the THD as a function of the number of frequencies components measured. We found that the strain noise was relatively constant provided at least 15 frequencies were measured. In addition, using at least 15 frequency components provided an average THD below −30 dB. While the standard deviation in the THD was relatively large, the upper end was still below −20 dB provided at least 15 frequencies were used. The simulations also indicated that if we were able to achieve a shot-noise limited measurement under these parameters, we could expect the sensor to exhibit a minimum detectable strain below 1 p$\varepsilon/\sqrt{\text{Hz}}$. In practice, a number of other noise sources could potentially limit the sensor performance, including laser phase noise, detector noise, and digitization noise. Nonetheless, the main conclusion of this simulation, that ~15 uncorrelated RBS measurements are sufficient to obtain a linear strain response, is independent of the source of the noise term in Eq. 3. Finally, since this is an amplitude-based approach, the sensor is naturally immune to noise due to interference fading.

Optics EXPRESS

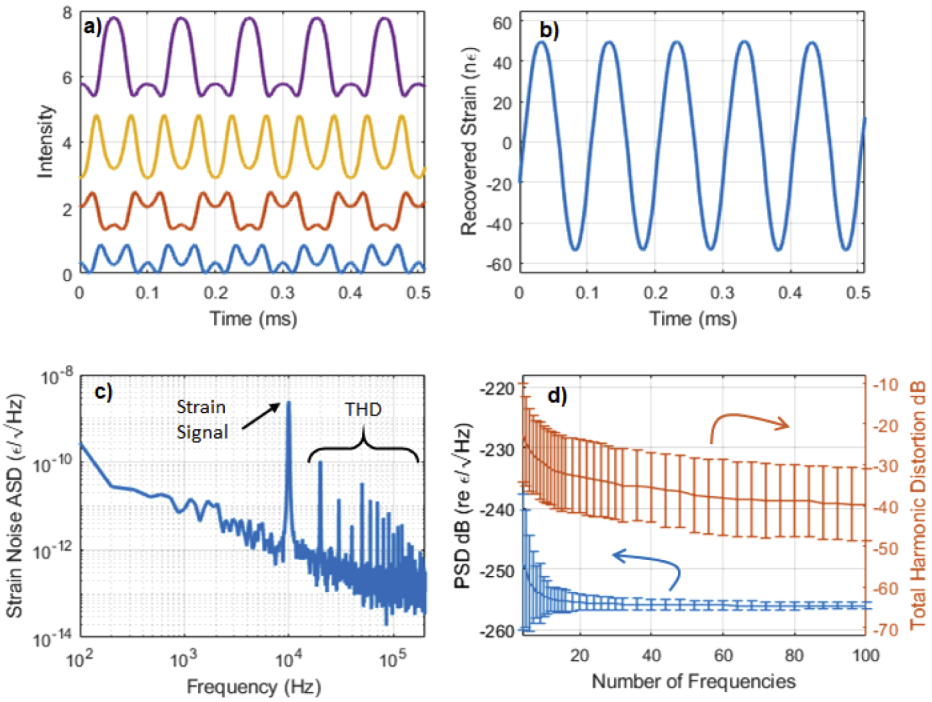

Fig. 2. (a) Simulated Rayleigh backscattered intensity under a 10 kHz sinusoidal strain for four uncorrelated frequencies. (b) Recovered strain obtained by combining information from 18 discrete frequency components. (c) The strain noise ASD showing the signal at 10 kHz and the higher harmonic contributions recovered using 18 frequency components. (d) The strain noise power spectral density (PSD) is shown as a function of the number of frequencies measured on the left axis. The right-axis shows the total harmonic distortion. The error bars indicate the standard deviation over 1000 simulations with randomly positioned scatterers.

4. Experimental demonstration

Based on the simulations presented above, we designed and constructed a φ-OTDR system capable of recording 18 uncorrelated RBS measurements in parallel. The interrogation system first generated an optical frequency comb consisting of 9 lines by modulating a single seed laser. In order to separately measure the RBS amplitude of each comb line, we combined the backscattered comb with a local oscillator (LO) and monitored the strength of the 9 interference signals. Additionally, by dividing the RBS light into orthogonal polarizations [23], we performed two sets of these interference measurements to provide a total of 18 uncorrelated RBS measurements from a single optical pulse.

A schematic of the experimental setup is shown in Fig. 3(a). Light from a narrowband (10 kHz linewidth) continuous wave laser operating at 1550 nm was divided into an interrogation arm and a reference arm or LO. The interrogation arm passed through an electro-optic intensity modulator which was driven with a digital frequency comb consisting of a sum of sinewaves at 60, 120, 180, and 240 MHz. The DC bias applied to the intensity modulator was adjusted to balance the power between the unshifted light at the original laser frequency and the four pairs of sidebands, resulting in a comb with 9 frequency lines each separated by 60 MHz. An acousto-optic modulator (AOM) operating at 54 MHz was then used to carve 100 ns (full-width at half-maximum) pulses at a repetition rate of 1 MHz. The pulses were amplified by an erbium doped fiber amplifier (EDFA) to an average power of 30 dBm before entering the fiber under

Optics EXPRESS

test. The fiber under test consisted of ~90 m of single mode fiber with the middle 9 m of fiber wrapped on a PZT tube. The RBS light was separated using a circulator before being amplified and spectrally filtered to remove the amplified spontaneous emission. Finally, the RBS light was combined with the LO and the two polarization states were separately detected using a pair of 600 MHz bandwidth photodetectors and digitized at 5 GS/s. The LO was frequency shifted by −216 MHz using AOMs and the polarization controller was adjusted to evenly distribute the LO power on the two photodetectors. The relative optical frequencies of the input comb and the LO are shown in Fig. 3(b), while Fig. 3(c) shows the relevant frequencies obtained by taking the Fourier transform of the interference signal recorded on the photodetectors. Note that the 60 MHz comb frequency spacing was larger than the frequency correlation width of the RBS spectrum for the 100 ns pulse duration used, ensuring that we acquired uncorrelated RBS measurements [24]. The LO frequency was selected so that the interference terms of interest (between the LO and the frequency comb) were spaced by 60 MHz between 30 MHz and 510 MHz and separated by 30 MHz from the self-interference terms of the comb. Using a strong LO relative to the comb also helped to suppress the influence of the self-interference terms.

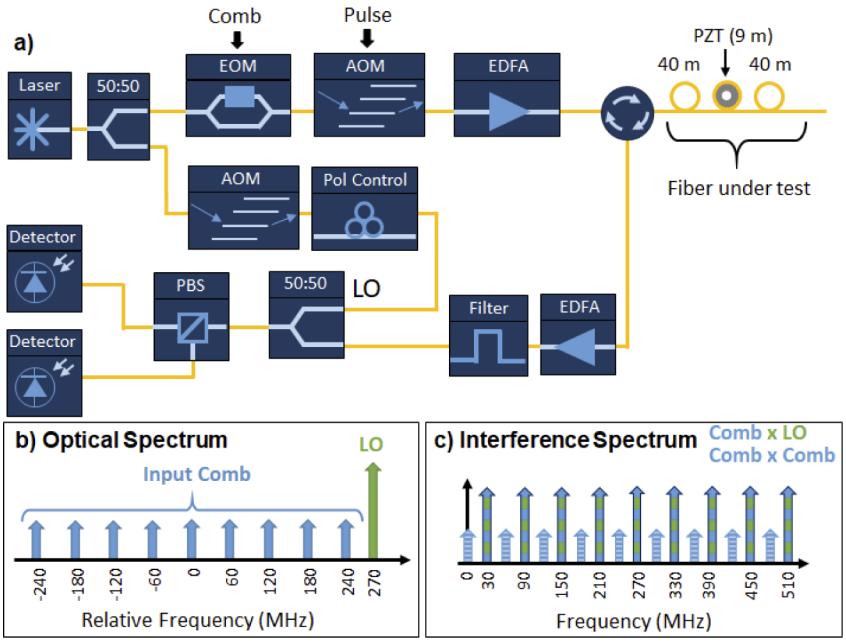

Fig. 3. (a) Experimental setup used to perform quantitative strain measurements. (b) The optical frequency comb used to probe the fiber under test consisted of 9 lines separated by 60 MHz while the LO was shifted by 270 MHz relative to the center of the frequency comb. (c) The electrical interference spectrum recorded on the photodetector included 9 interference terms between the comb lines and the LO indicated in blue and green along with a series of self-interference terms between the various comb lines. The LO frequency was selected to maximize the separation between the desired interference terms and the self-interference terms.

Although the system used interferometric detection to demultiplex the frequency components, we only required the amplitude of the RBS light at each frequency to recover the fiber strain. This significantly relaxes the laser phase noise requirements since the relative phase between the LO and the RBS light was discarded.

A typical interference pattern recorded using this experimental setup is shown in Fig. 4(a). In order to recover the strain, we first performed short-time Fourier transforms (STFT) on 100

Optics EXPRESS

ns segments of the raw data to extract the amplitude of the 9 frequency components in each polarization state. A typical STFT spectrum is shown in Fig. 4(b). The STFT frequency bin size is 10 MHz (set by the 100 ns pulse duration) allowing us to easily resolve the comb teeth. We repeated this process for each pulse to extract the evolution of the RBS amplitude at each frequency over time. This provided a matrix consisting of the 18 RBS realizations over time, as shown in Fig. 4(c). The RBS amplitude of four of these frequency components recorded while the PZT was driven with a 1 kHz sinusoidal modulation with an amplitude of 220 nε is shown in Fig. 4(d).

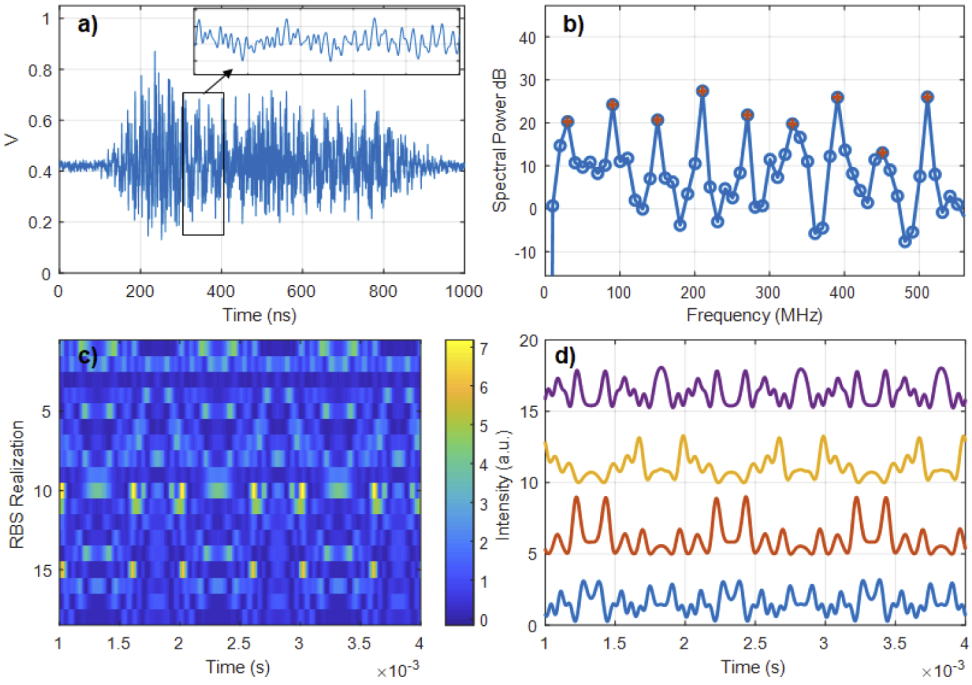

Fig. 4. (a) A typical unprocessed interference pattern recorded on one of the photodetectors. This type of interference pattern is recorded at the pulse repetition rate of 1 MHz. (b) The Fourier transform of a 100 ns segment of the measured interference pattern. The interference frequencies produced by the nine comb lines beating with the LO are indicated in orange. (c) The extracted RBS amplitude for the 18 realizations is shown as a function of time under a sinusoidal strain. (d) Cross sections of four RBS realizations shown under a sinusoidal strain.

By selecting different 100 ns segments in the interference pattern relative to the time when each pulse entered the fiber under test, we were able to extract the strain at varying positions in the fiber, providing a fully distributed measurement. In the following, we focus on the strain measured at the center of the fiber under test where the PZT was located.

After extracting the RBS amplitude for the 9 frequency components at each polarization, we applied the strain recovery algorithm previously developed for a multimode fiber [19]. Figures 5(a) and 5(b) show the recovered strain when the PZT was subjected to a 200 Hz sinusoidal and sawtooth drive. The sensor is able to clearly differentiate between the two waveforms. To quantitatively evaluate the linearity of the sensor, we applied a 10 kHz signal to the PZT and calculated the THD. The sensor exhibited a THD below −35 dB with a minimum detectable strain in the 1 to 9 kHz band of 5 p$\varepsilon/\sqrt{\text{Hz}}$, as shown in Fig. 5(c).

Optics EXPRESS

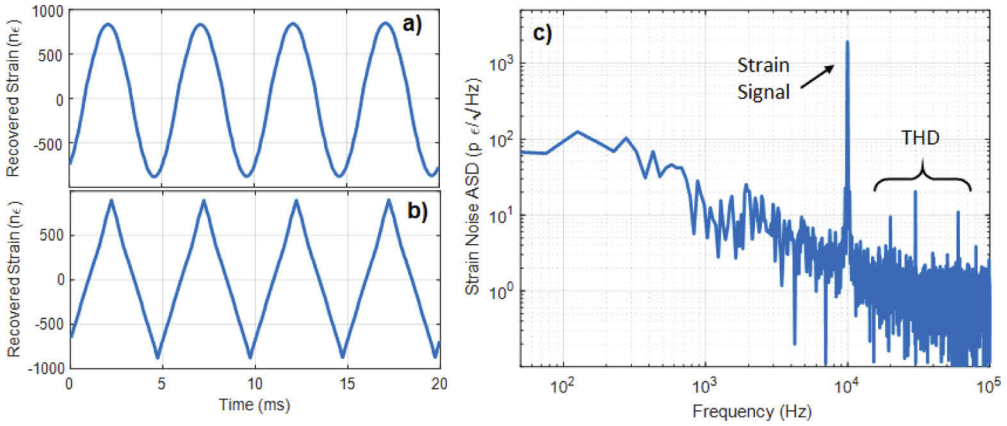

Fig. 5. Experimentally measured strain under a 200 Hz sinusoidal (a) and sawtooth (b) modulation. (b) Minimum detectable strain noise measured with a 10 kHz sinusoidal modulation applied to the PZT. The average strain noise between 1 and 9 kHz is 5 $p\varepsilon/\sqrt{Hz}$ and the THD is below −35 dB.

5. Conclusion

In summary, we presented an amplitude measuring φ-OTDR technique capable of performing quantitative strain measurements. The approach relies on computationally recovering the strain from a series of uncorrelated RBS patterns. We performed simulations indicating that a linear strain response (average THD below −30 dB) could be achieved with as few as 15 uncorrelated RBS patterns. We then introduced a modified φ-OTDR system which used a combination of frequency and polarization multiplexing to record 18 uncorrelated RBS patterns in parallel. We experimentally measured a series of strain signals and showed that the sensor can differentiate between sawtooth and sinusoidal strains. The sensor exhibited a minimum detectable strain of 5 $p\varepsilon/\sqrt{Hz}$ and a THD below −35 dB. The sensor bandwidth is limited only by the roundtrip lifetime in the fiber and the detection scheme is naturally immune to signal fading.

Funding

U.S. Naval Research Laboratory.

Disclosures

The authors declare no conflicts of interest.

References

1. A. Masoudi and T. P. Newson, "Contributed Review: Distributed optical fibre dynamic strain sensing," Rev. Sci. Instrum. **87**(1), 011501 (2016).
2. J. C. Juarez and H. F. Taylor, "Field test of a distributed fiber-optic intrusion sensor system for long perimeters," Appl. Opt. **46**(11), 1968–1971 (2007).
3. F. Peng, H. Wu, X.-H. Jia, Y.-J. Rao, Z.-N. Wang, and Z.-P. Peng, "Ultra-long high-sensitivity Φ-OTDR for high spatial resolution intrusion detection of pipelines," Opt. Express **22**(11), 13804–13810 (2014).
4. C. K. Kirkendall and A. Dandridge, "Overview of high performance fibre-optic sensing," J. Phys. D: Appl. Phys. **37**(18), R197–R216 (2004).
5. J. P. Dakin and C. Lamb, "Distirbuted Fibre Optic Sensor System,"GB patent No. 2222247A (1990).
6. R. Posey, G. A. Johnson, and S. T. Vohra, "Strain sensing based on coherent Rayleigh scattering in an optical fibre," Electron. Lett. **36**(20), 1688–1689 (2000).
7. A. Masoudi, M. Belal, and T. P. Newson, "A distributed optical fibre dynamic strain sensor based on phase-OTDR," Meas. Sci. Technol. **24**(8), 085204 (2013).

Optics EXPRESS

8. H. Liu, F. Pang, L. Lv, X. Mei, Y. Song, J. Chen, and T. Wang, "True Phase Measurement of Distributed Vibration Sensors Based on Heterodyne φ-OTDR," IEEE Photonics J. **10**(1), 1–9 (2018).
9. M. Chen, A. Masoudi, and G. Brambilla, "Performance analysis of distributed optical fiber acoustic sensors based on φ-OTDR," Opt. Express **27**(7), 9684–9695 (2019).
10. J. Zhou, Z. Pan, Q. Ye, H. Cai, R. Qu, and Z. Fang, "Characteristics and Explanations of Interference Fading of a φ-OTDR With a Multi-Frequency Source," J. Lightwave Technol. **31**(17), 2947–2954 (2013).
11. M. Zabihi, Y. Chen, T. Zhou, J. Liu, Y. Shan, Z. Meng, F. Wang, Y. Zhang, X. Zhang, and M. Chen, "Continuous Fading Suppression Method for Φ-OTDR Systems Using Optimum Tracking Over Multiple Probe Frequencies," J. Lightwave Technol. **37**(14), 3602–3610 (2019).
12. S. Liehr, Y. S. Muanenda, S. Münzenberger, and K. Krebber, "Relative change measurement of physical quantities using dual-wavelength coherent OTDR," Opt. Express **25**(2), 720–729 (2017).
13. S. Liehr, S. Münzenberger, and K. Krebber, "Wavelength-scanning coherent OTDR for dynamic high strain resolution sensing," Opt. Express **26**(8), 10573–10588 (2018).
14. Y. Koyamada, M. Imahama, K. Kubota, and K. Hogari, "Fiber-optic distributed strain and temperature sensing with very high measurand resolution over long range using coherent OTDR," J. Lightwave Technol. **27**(9), 1142–1146 (2009).
15. L. Zhou, F. Wang, X. Wang, Y. Pan, Z. Sun, J. Hua, and X. Zhang, "Distributed strain and vibration sensing system based on phase-sensitive OTDR," IEEE Photonics Technol. Lett. **27**(17), 1884–1887 (2015).
16. J. Pastor-Graells, H. F. Martins, A. Garcia-Ruiz, S. Martin-Lopez, and M. Gonzalez-Herraez, "Single-shot distributed temperature and strain tracking using direct detection phase-sensitive OTDR with chirped pulses," Opt. Express **24**(12), 13121–13133 (2016).
17. M. R. Fernańdez-Ruiz, J. Pastor-Graells, H. F. Martins, A. Garcia-Ruiz, S. Martin-Lopez, and M. Gonzalez-Herraez, "Laser Phase-Noise Cancellation in Chirped-Pulse Distributed Acoustic Sensors," J. Lightwave Technol. **36**(4), 979–985 (2018).
18. D. Chen, Q. Liu, Y. Wang, H. Li, and Z. He, "Fiber-optic distributed acoustic sensor based on a chirped pulse and a non-matched filter," Opt. Express **27**(20), 29415–29424 (2019).
19. M. J. Murray, A. Davis, C. Kirkendall, and B. Redding, "Speckle-based strain sensing in multimode fiber," Opt. Express **27**(20), 28494–28506 (2019).
20. M. Nakazawa, "Rayleigh backscattering theory for single-mode optical fibers," J. Opt. Soc. Am. **73**(9), 1175–1180 (1983).
21. D. Chen, Q. Liu, X. Fan, and Z. He, "Distributed Fiber-Optic Acoustic Sensor with Enhanced Response Bandwidth and High Signal-to-Noise Ratio," J. Lightwave Technol. **35**(10), 2037–2043 (2017).
22. P. Healey, "Fading in heterodyne OTDR," Electron. Lett. **20**(1), 30–32 (1984).
23. J. C. Juarez and H. F. Taylor, "Polarization discrimination in a phase-sensitive optical time-domain reflectometer intrusion-sensor system," Opt. Lett. **30**(24), 3284–3286 (2005).
24. M. D. Mermelstein, R. Posey, G. A. Johnson, and S. T. Vohra, "Rayleigh scattering optical frequency correlation in a single-mode optical fiber," Opt. Lett. **26**(2), 58–60 (2001).